Magnetic properties of nanocomposite Fe-doped SBA15 magnetic materials

ARTICLE *in* MATERIALS CHEMISTRY AND PHYSICS · NOVEMBER 2008

Impact Factor: 2.13 · DOI: 10.1016/j.matchemphys.2008.05.019

11 AUTHORS, INCLUDING:

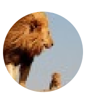

Yapi Liu
China Jiliang University

Hengming Ge
Jiangsu Provincial Center for Disease Contr…

X. Q. Wang
China Jiliang University

Materials Chemistry and Physics 112 (2008) 112–114

Contents lists available at ScienceDirect

Materials Chemistry and Physics

journal homepage: www.elsevier.com/locate/matchemphys

Magnetic properties of nanocomposite Fe-doped SBA-15 magnetic materials

H.X. Jin, L. Li, N.J. Chu, Y.P. Liu, L.Y. Wang, Q. Lu, J. Qian, L.N. Sun, Q. Tang, H.L. Ge, X.Q. Wang*

Zhejiang Province Key Laboratory of Magnetism, School of Materials Science and Engineering, China Jiliang University, Hangzhou 310018, China

ARTICLE INFO

Article history:
Received 5 April 2008
Received in revised form 12 May 2008
Accepted 14 May 2008

Keywords:
Magnetic materials
Sol–gel growth
Microstructure
Magnetic properties

ABSTRACT

Fe-doped SBA-15 magnetic materials was synthesized by pH-adjusting method, and then characterized by X-ray diffraction (XRD) and vibrating sample magnetometer (VSM). All results showed that the samples presented ferromagnetism and the magnetism improved with the Fe content. Saturation magnetization and coercivity of the as-prepared Fe-doped SBA-15 samples increased with the calcined temperature up to 850 °C, followed by decreasing. Furthermore, the magnetic properties at lower temperature (measured at 100 K) of the Fe-doped samples was presented. Finally, the type of the intergranular exchange interaction was conformed by plotting Henkel (δM) formulation.

1. Introduction

Magnetic nanoparticles were of great interest for researchers from different fields, including magnetic fluids, catalysis, biotechnology/biomedicine, magnetic resonance imaging, data storage, and environmental remediation [1–4]. Since successful application of such magnetic nanoparticles was highly dependent on the stability of the particles under a range of different conditions, a number of suitable methods had been developed for the synthesis of magnetic nanoparticles with various compositions.

SBA-15 was a mesoporous silica molecular sieve with high surface area, tunable uniform hexagonal channels (5–30 nm) and thick framework walls (3–6 nm), which was therefore thermally and hydrothermally robust [5–6]. With very large pores, thick pore walls, and superior hydrothermal stability, SBA-15 had the promising applications in many fields for the preparation of nanomaterials, catalysis, separation, adsorption [7–10]. The perfect periodic of nanotube array enabled SBA-15 to serve as nanoreactors, which provided an effective way to controlling the uniformity of nanoparticle size and preventing agglomeration of the nanoparticles.

Many researches focused on the magnetic properties of SBA-15 mesoporous magnetic materials, such as Fe_3O_4, Fe_2O_3, FePt, Co_3O_4 and so on [11–17]. A site-selective delivery system for controlled drug release was fabricated, which the magnetization (Ms) was about 0.8 emu g^{-1} [11]. Paramagnetic α-Fe_2O_3 nanoparticles were synthesized by thermolysis of $Fe(NO_3)_3$ inside the pores of SBA-15, which partial occupation of pores resulted in decrease of specific surface and the pore volume, giving rise to materials containing about 25% of Fe_2O_3 [12]. Delahaye described the use of mesoporous SBA-15 silica as hard templates for the size-controlled synthesis of Fe_3O_4 nanoparticles, and further discussed their magnetic property [13]. Kockrick et al. [14] had demonstrated the efficient generation of FePt nanoparticles in an ordered mesoporous oxide and subsequent transformation of the cubic FePt nanoparticles into fct-FePt. Ferromagnetic tetragonal FePt was obtained with a particle size predefined by the pore diameter of the matrix. The SBA-15 with ordered mesopore may be a valuable host for the generation of periodic nanomagnet assemblies.

In the previous works [15], we had proved the Fe_xO_y/SBA-15 magnetic materials present ferromagnetism. In this paper, the preparation of the Fe-doped SBA-15 was similar to the method mentioned in the previous paper with the different Fe content. Using X-ray diffraction (XRD), Fe_2O_3 nanoparticles were confirmed in the surface of SBA-15. Furthermore, the magnetic properties of the as-prepared Fe-doped SBA-15 were measured by vibrating sample magnetometer (VSM). Finally, the type of the intergranular exchange interaction was characterized by plotting Henkel (δM) formulation.

2. Experimental

The preparation of the precursor solutions of the Fe-doped SBA-15 magnetic materials was similar to the process mentioned in literature [15]. Briefly, 2 g surfactants (Pluronic P_{123}, $(EO)_{20}(PO)_{70}(EO)_{20}$), 60 ml 2 M HCl, 15 ml de-ioned water, 4.5 ml tetraethoxysilane (TEOS) and iron nitrate ($Fe(NO)_3{\cdot}9H_2O$) were mixed together, then the pH value of solution was adjusted at about 7 by ammonia. We assumed % by wt Fe_2O_3 from preparative recipe since $Fe(NO_3)_3$ changed into $Fe(OH)_3$ completely when pH was adjusted to 7. After the mixture hydrothermal treated for 2 days, the

* Corresponding author at: School of Materials Science and Engineering, China Jiliang University, Hangzhou 310018, China. Tel.: +86 571 8683 5609.
E-mail address: wxqnano@cjlu.edu.cn (X.Q. Wang).

0254-0584/$ – see front matter © 2008 Elsevier B.V. All rights reserved.
doi:10.1016/j.matchemphys.2008.05.019

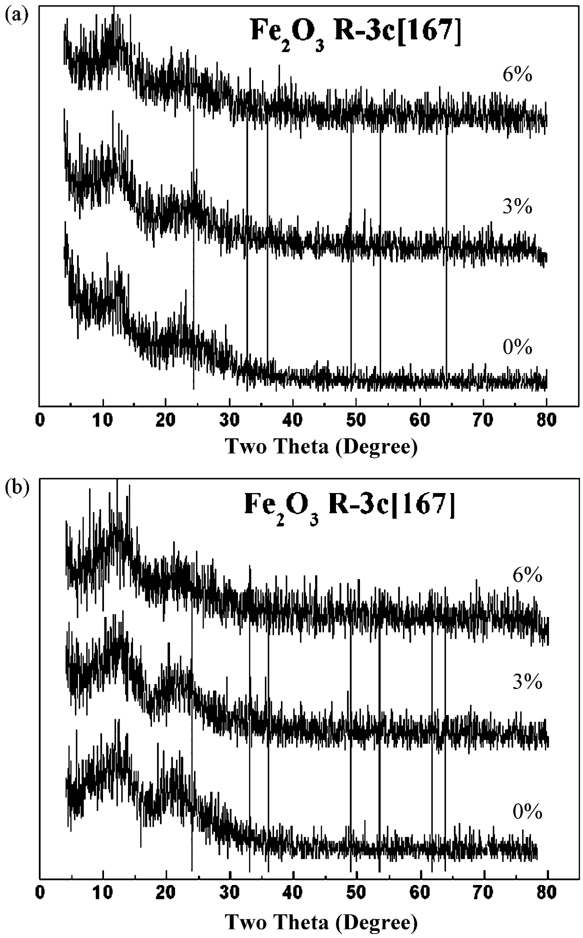

Fig. 1. XRD patterns of Fe-doped SBA-15 calcined at 550 °C (a) and 950 °C (b) in air.

as-prepared powders were calcined at the different temperature and thereby the solids of the Fe-doped SBA-15 were obtained.

Using XRD (XD-5A, Cu target, wavelength 0.154 nm), the microstructure of the calcined samples was characterized. VSM (LakeShore-7407, 2T) was introduced to study the magnetic properties of the Fe-doped SBA-15.

3. Results and discussion

As mentioned in our previous paper [7], the Fe could not occupy the mesopore since they were filled with surfactants and the Fe should anchor in the frame or surface of SBA-15. The thermal stability was improved with Fe loading [7]. Herein, wide-angle XRD patterns of the Fe-doped SBA-15 were given in Fig. 1, which included the calcined temperature of 550 °C (a) and 950 °C (b). The very-wide diffraction peaks for amorphous solid of silica were found at 8–18° and 20–30°. Compared with the pure SBA-15, the peaks of Fe_2O_3 with the structure of hematite (space group: *R*-3*c*[167]) for the Fe-doped SBA-15 were detected faintly at high scanning angle, which indicated that Fe_2O_3 existed in nanoparticles and were well dispersed in SBA-15.

Furthermore, the magnetic properties of the as-prepared SBA-15 with the different Fe content were characterized by VSM in Figs. 2 and 3. From the above hysteresis loops, it could be concluded the addition of Fe_2O_3 nanoparticles led to the as-prepared SBA-15 presented the ferromagnetic properties. In Figs. 2 and 3, coercivity of the Fe-doped SBA-15 increased with the calcined temperature up to 850 °C with the maximum value of 390 Oe for 3% Fe-doped SBA-15 and 590 Oe for 6% Fe-doped SBA-15. These values were larger than coercivity of 330 Oe for the single-domain with and

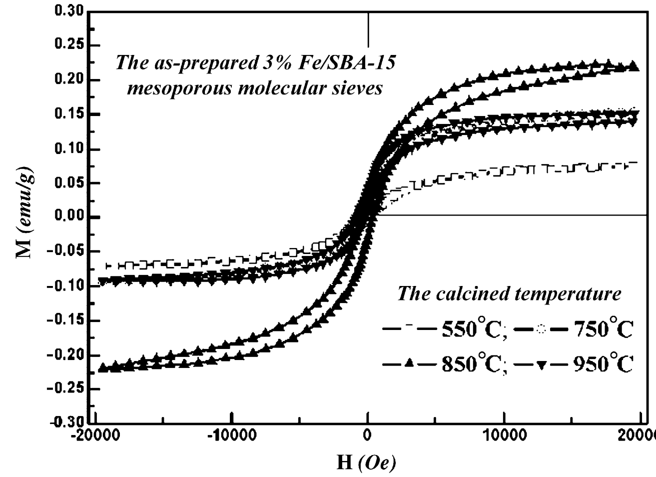

Fig. 2. Hysteresis loops of 3% Fe-doped SBA-15 calcined at different temperature.

150 Oe for the multi-domain of Fe_2O_3 magnetic materials, and it should be attributed to the exchange interaction between the Fe_2O_3 nanoparticles.

The effective way to prove the existence of exchange-coupling interaction was to measure the Henkel plots (δM) of specimens [18,19]: $\delta M = M_d(H)/M_r(\infty) - [1 - 2M_r(H)/M_r(\infty)]$, where $M_d(H)$ was the reduced DC demagnetization remanence and $M_r(H)$ was the reduced isothermal remanent magnetization. The profile of the $\delta M(H)$ curve could reveal the different contribution of magnetostatic interaction and exchange interaction. The $\delta M(H)$ plot was predicted to be negative for a pure magnetostatic interaction, and a positive $\delta M(H)$ could confirm the addition of exchange interaction. The value of δM could present the intensity of the interaction between the particles. The $\delta M(H)$ curves of the as-prepared Fe-doped SBA-15 calcined at 850 °C were shown in Fig. 4. The positive value of δM indicated the existence of the exchange interaction between the Fe_2O_3 nanoparticles in the frame of SBA-15. The value of δM increased with the applied field, which indicated the exchange interaction became stronger. The larger coercivity of Fe-doped SBA-15 samples should be attributed to the exchange interaction between the Fe_2O_3 nanoparticles.

For magnetic nanoparticles, coercivity was maximal with the diameter of the magnetic single-domain size. When the diameter was larger than the supermagnetism critical dimension and

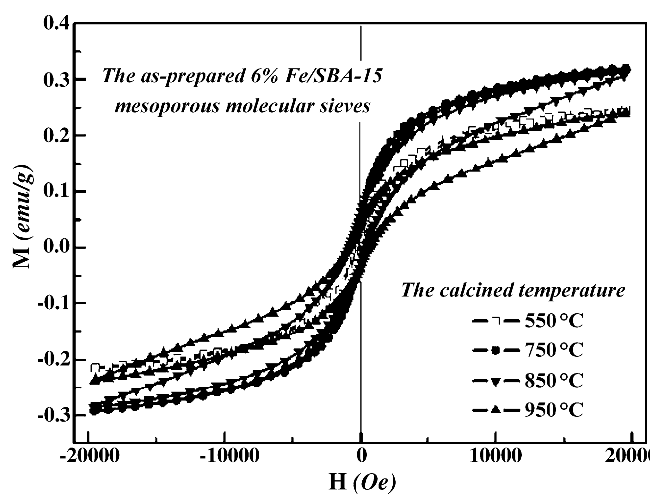

Fig. 3. Hysteresis loops of 6% Fe-doped SBA-15 calcined at different temperature.

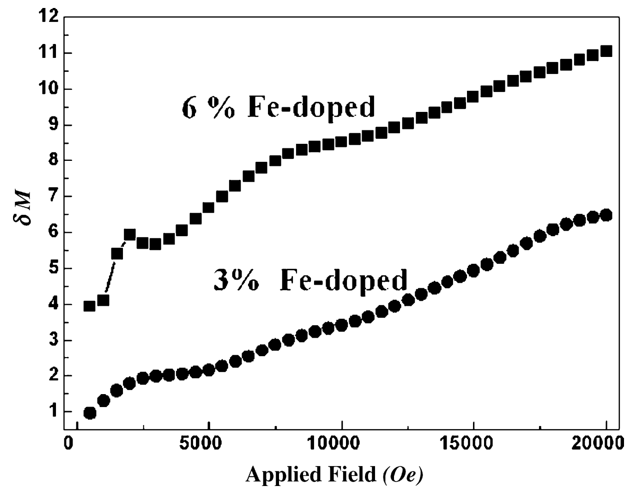

Fig. 4. δM curves of Fe-doped SBA-15 calcined at 850 °C.

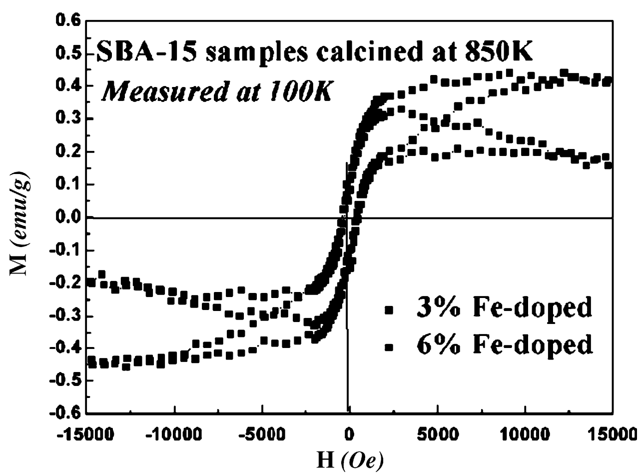

Fig. 5. Fe-doped SBA-15 hysteresis loops measured at 100 K.

was lower than the single-domain size, coercivity increased with the size of nanoparticles. For the as-prepared Fe-doped SBA-15 magnetic materials, the Fe_2O_3 diameter was larger than the super-magnetism critical dimension and was smaller than the magnetic single-domain size. As the results, coercivity of the Fe-doped SBA-15 increased with the diameter of Fe_2O_3 nanoparticles. With the increasing calcined temperature, the Fe_2O_3 nanoparticles grew up by degrees when the temperature was lower than 850 °C. When the calcined temperature was higher than 850 °C, partial micropore in SBA-15 collapsed, which made Fe_2O_3 nanoparticles assemble easilier [7]. The larger Fe_2O_3 crystal grains and the higher calcined temperature both given rise to the better crystallization, which decreased the magnetocrystalline anisotropy of magnetic materials. As the results, coercivity decreased to some extent. Therefore, coercivity of the Fe-doped SBA-15 increased with the calcined temperature up to 850 °C, followed by decreasing. With the higher Fe content, the larger diameter of Fe_2O_3 nanoparticles was close to the single-domain size. Thus, the 6% Fe-doped SBA-15 had the larger coercivity than the 3% samples.

Owning to the low content of Fe_2O_3 nanoparticles, saturation magnetization (Ms) was smaller than usual materials. The trend of Ms was the same with coercivity, and increased with the calcined temperature up to 850 °C. Usually, Ms increased with the Fe density in the sample, and Ms of the 6% Fe-doped SBA-15 was higher than that of 3% Fe-doped SBA-15. The density of the as-prepared SBA-15 was too small to be presser bit hardly, which maybe influence the measurement of magnetic properties.

Furthermore, the magnetic properties of the as-prepared Fe-doped SBA-15 calcined at 850 °C were measured at 100 K, which was given in Fig. 5. In any case, the thermal disturbance of the magnetic moment weakened with the decreasing measurement temperature, as the results, coercivity and Ms of the samples should increase to some extent. Compared with the magnetic properties measured at the room temperature, Ms at 100 K increased from 0.22 to 0.31 emu g^{-1} for 3% Fe-doped SBA-15 and from 0.32 to 0.43 emu g^{-1} for 6% Fe-doped sample. Coercivity of the 3% Fe-doped SBA-15 increased a little from 390 Oe to 440 Oe. But for 6% Fe-doped sample, the coercive decreased from 590 Oe to 580 Oe, which should be further confirmed in later work.

4. Conclusions

Fe-doped SBA-15 magnetic materials were prepared in two-step method. The results showed that all the samples had the well-ordered hexagonal mesoporous structures and Fe_2O_3 nanoparticles pinned in the surface of the SBA-15. The magnetic properties increased with increasing calcined temperature, and the maximum was obtained at 850 °C. The δM curves proved that the exchange interaction between Fe_2O_3 nanoparticles.

Acknowledgements

The research is funded by National Natural Science Foundation of China (10647149, 20571067 and 20601024).

References

[1] S.C. Tsang, V. Caps, I. Paraskevas, D. Chadwick, D. Thompsett, Angew. Chem. 116 (2004) 5763.
[2] A.K. Gupta, M. Gupta, Biomaterials 26 (2005) 3995.
[3] S. Mornet, S. Vasseur, F. Grasset, P. Verveka, G. Goglio, A. Demourgues, J. Portier, E. Pollert, E. Duguet, Prog. Solid State Chem. 34 (2006) 237.
[4] Z. Li, L. Wei, M.Y. Gao, H. Lei, Adv. Mater. 17 (2005) 1001.
[5] D.Y. Zhao, J.L. Feng, Q.S. Huo, N. Melosh, G.H. Fredrickson, B.F. Chmelka, G.D. Stucky, Science 279 (1998) 548.
[6] M. Gomez-Cazalilla, J.M. Merida-Robles, A. Gurbani, E. Rodrıguez-Castellon, A. Jimenez-Lopez, J. Solid State Chem. 180 (2007) 1130.
[7] X.Q. Wang, H.L. Ge, H.X. Jin, Y.J. Cui, Micropor. Mesopor. Mater. 86 (2005) 335.
[8] X.Q. Wang, M. Wang, H.X. Jin, Z.H. Li, P.M. He, Appl. Surf. Sci. 243 (2005) 151.
[9] H. Song, R.M. Rioux, J.D. Hoefelmeyer, R. Komor, K. Niesz, M. Grass, P. Yang, G.A. Somorjai, J. Am. Chem. Soc. 128 (2006) 3027.
[10] D. Srinivas, P. Ratnasamy, Micropor. Mesopor. Mater. 105 (2007) 170.
[11] S.M. Zhu, Z.Y. Zhou, D. Zhang, Chem. Phys. Chem. 8 (2007) 2478.
[12] F. Jiao, B. Yue, K. Zhu, D. Zhao, H. He, Chem. Lett. 32 (2003) 770.
[13] E. Delahaye, V. Escax, N. Ei Hassan, A. Davidson, R. Aquino, V. Dupuis, R. Perzynski, Y.L. Raikher, J. Phys. Chem. B 110 (2006) 26001.
[14] E. Kockrick, P. Krawiec, W. Schnelle, D. Geiger, F.M. Schappacher, R. Pöttgen, S. Kaskel, Adv. Mater. 19 (2007) 3021–3026.
[15] L. Li, N.J. Chu, H.X. Jin, H.L. Ge, X.Q. Wang, Chin. J. Inorg. Chem. 23 (2007) 1753 (in Chinese).
[16] J.-S. Jung, K.-H. Choi, Y.-K. Jung, S.H. Lee, V.O. Golub, L. Malkinski, C.J. O'Connor, J. Magn. Magn. Mater. 272–276 (2004) e1157–e1159.
[17] S.X. Liu, B. Yue, K. Jiao, Y. Zhou, H.Y. He, Mater. Lett. 60 (2006) 154.
[18] E.P. Wohlfarth, J. Appl. Phys. 29 (1958) 595.
[19] P.E. Kelly, K. O'Grady, P.I. Hayo, R.W. Chantrell, IEEE Trans. Magn. 25 (1989) 3881.